Calculation of Geopotential and Temperature Fields from an Array of Nearly Continuous Wind Observations

YING-HWA KUO AND RICHARD A. ANTHES

National Center for Atmospheric Research,[1] Boulder, CO 80307

(Manuscript received 11 June 1984, in final form 4 October 1984)

ABSTRACT

Observing systems simulation experiments were carried out to estimate the accuracy of temperatures diagnosed from the divergence equation when an array of nearly continuous (in time) wind observations is available. It was found that a useful estimate of temperature can be derived from high-resolution wind observations such as those obtainable from a network of wind profiling systems. Adding the divergence and vertical motion terms to the balance equation to form the complete divergence equation reduces the errors in derived temperatures and geopotential heights. Observations on an irregularly spaced grid lead to greater errors than those on a regularly spaced grid. Moderate errors are also introduced when large-scale errors in geopotential occur in the lateral boundary conditions. This suggests the need for some independent observations of temperature (from rawinsonde or temperature profiler) to prescribe the boundary conditions for the retrieval technique.

In a simulation of a possible operational system in which wind observations with random errors of 1 m s^{-1} are available on a 350 km grid and boundary values of geopotential height contain errors typical of a 12 h model forecast, the derived temperatures and heights on the interior of the grid contain root-mean-square errors of 1.55°C and 18.8 m, respectively.

1. Introduction

The recent development of the wind Profiler, a ground-based Doppler radar system that provides high (every few minutes) temporal resolution vertical profiles of the horizontal wind, represents a breakthrough in wind-sounding technology (Hogg *et al.*, 1983; Strauch *et al.*, 1984). The nearly continuous wind soundings, with an accuracy equal to or better than rawinsondes, offer many opportunities in research and operational meteorology (Hovermale, 1983; Shapiro *et al.*, 1983). Data processing and analysis techniques, such as temporal filtering and time-to-space conversions, promise to yield horizontal wind analyses with accuracies much better than possible in the past; in particular, it is likely that meaningful fields of temporally continuous horizontal divergence (Zamora and Shapiro, 1984) and derived vertical motion can be estimated in real time. The fields of vertical motion may prove useful in short-range forecasting if, as suggested by research studies (e.g., Ogura, 1975), low-level mesoscale convergence precedes the outbreak of convective precipitation, as well as in diagnostic research studies which often require accurate, independent estimates of vertical velocity (for example, budget studies of heat, moisture, vorticity, or kinetic energy).

Another potential use of temporally continuous analyses of horizontal divergence is in the initialization of numerical weather prediction models. Not only could the divergent component of the wind be provided directly to numerical models, but the analysis of divergence may also be useful in estimating the temperature structure through the diagnostic divergence equation (Fankhauser, 1974; Bleck *et al.*, 1984). This equation relates the geopotential field to the horizontal wind field and includes terms involving the divergence, its temporal rate of change, and the vertical velocity. After the geopotential has been found, the temperatures may be calculated from the hydrostatic equation. While it is unlikely that the need for some independent measurements of temperature will be eliminated, the derived temperatures may provide useful supplementary information to improve the temperature analysis.

This paper investigates the accuracy of temperature estimates derived from the divergence equation when wind observations of various spatial and temporal resolutions and accuracies are available. The basic data set used in this study is the high-resolution model data set used by Kuo and Anthes (1984a) in observing systems simulation experiments (OSSE) designed to estimate the errors in heat and moisture budgets (Kuo and Anthes, 1984b) calculated from

[1] The National Center for Atmospheric Research is sponsored by the National Science Foundation.

the AVE-SESAME-1979 special observational network. This model data set is modified in ways to simulate wind observations that appear feasible from an operational network of wind Profilers.

2. Theory and computational procedures

a. The divergence equation

Because the Profiler OSSEs are done on a Lambert Conformal Map Projection, the divergence equation is derived from the equation of motion on that projection,

$$\frac{\partial u}{\partial t} + mu\frac{\partial u}{\partial x} + mv\frac{\partial u}{\partial y} + \omega\frac{\partial u}{\partial p} - fv = -m\frac{\partial \phi}{\partial x} + F_u, \tag{1}$$

$$\frac{\partial v}{\partial t} + mu\frac{\partial v}{\partial x} + mv\frac{\partial v}{\partial y} + \omega\frac{\partial v}{\partial p} + fu = -m\frac{\partial \phi}{\partial y} + F_v, \tag{2}$$

where u and v are the horizontal wind components in the west–east and south–north directions respectively, ω is the vertical velocity in pressure coordinates (dp/dt), f the Coriolis parameter, ϕ the geopotential, m the map-scale factor, and F_u and F_v represent frictional and other subgrid-scale effects. In the numerical model used to generate the data set used in the OSSE, F_u and F_v are modeled at all levels according to

$$F_u = -K\nabla^4 u,$$
$$F_v = -K\nabla^4 v, \tag{3}$$

with an additional term representing surface drag in the lowest level of the model. By differentiating (1) with respect to x and (2) with respect to y, the divergence equation is obtained:

$$\frac{\partial D}{\partial t} + m^2\left(u\frac{\partial D'}{\partial x} + v\frac{\partial D'}{\partial y}\right) + m^2(D')^2 + 2m^2\left(\frac{\partial v}{\partial x}\frac{\partial u}{\partial y} - \frac{\partial u}{\partial x}\frac{\partial v}{\partial y}\right) + \omega\frac{\partial D}{\partial p} + m\left(\frac{\partial \omega}{\partial x}\frac{\partial u}{\partial p} + \frac{\partial \omega}{\partial y}\frac{\partial v}{\partial p}\right) - m\gamma v + m\beta u - f\zeta = -m^2\nabla^2\phi + m^2\left(\frac{\partial F_u/m}{\partial x} + \frac{\partial F_v/m}{\partial y}\right), \tag{4}$$

where

$$D \equiv m^2\nabla\cdot\mathbf{V}/m, \tag{5}$$

$$D' \equiv \nabla\cdot\mathbf{V}, \tag{6}$$

$$\zeta = m^2\left(\frac{\partial v/m}{\partial x} - \frac{\partial u/m}{\partial y}\right), \tag{7}$$

$$\gamma = \frac{\partial f}{\partial x}, \quad \beta = \frac{\partial f}{\partial y}. \tag{8}$$

With analyses of both the divergent and rotational wind components available at frequent intervals (e.g., 1 h), all the terms on the left side of (4) may be estimated by finite differences. If the frictional terms on the right side of (4) are neglected, the geopotential ϕ may be solved over a region, given values of ϕ around the lateral boundaries of the domain. The frictional terms are probably small above the planetary boundary layer (PBL). While it might be possible to account for real frictional effects in the atmospheric PBL through the bulk aerodynamic relation, it is unlikely that realistic estimates of unresolvable scales of motion (turbulence) in the free atmosphere can be calculated from atmospheric data. In the model, the parameterization of these effects given by (3) is designed mainly to control the growth of very small-scale noise rather than to model real atmospheric processes. In the calculations in this paper all frictional terms are ignored.

Neglect of the divergence and vertical velocity terms in (4) yields the balance equation. Anthes and Keyser (1979) used the balance equation to derive temperatures in their initialization of a six-layer numerical model. They found root-mean-square (rms) differences between the derived temperatures and independently analyzed temperatures of between 2 and 4°C in the lower troposphere (1,000–700 mb), about 1.5°C in the middle troposphere (400–700 mb), and between 2.0 and 3.0°C in the upper troposphere (about 200 mb). They attributed the large errors in the lower troposphere to neglect of friction, and in the upper troposphere to the coarse vertical resolution in resolving the high stability. In addition to these effects, the neglect of horizontal divergence, which is usually largest in the lower and upper troposphere, may have contributed to these errors.

b. The data set

The data set used in these OSSEs was produced by a mesoscale model described by Anthes *et al.* (1982) and Kuo and Anthes (1984a). The model consists of ten evenly-spaced layers (Fig. 1) and has a horizontal resolution of 50 km. The model domain is centered over Oklahoma (Fig. 2). Frictional effects in the PBL are considered by the bulk aerodynamic method. Both stable precipitation and convective precipitation are parameterized. The model was initialized at 1200 GMT 10 April 1979 and the simulation carried out for 24 h.

Because the model simulation contains high temporal frequency variations which are not considered realistic, all model data were filtered to eliminate oscillations with periods less than 6 h. This procedure, described and illustrated fully by Kuo and Anthes (1984a), yields a slowly varying, dynamically consistent data set. The horizontal wind components from this data set are used to estimate the terms on the left side of (4) to calculate the geopotential. The

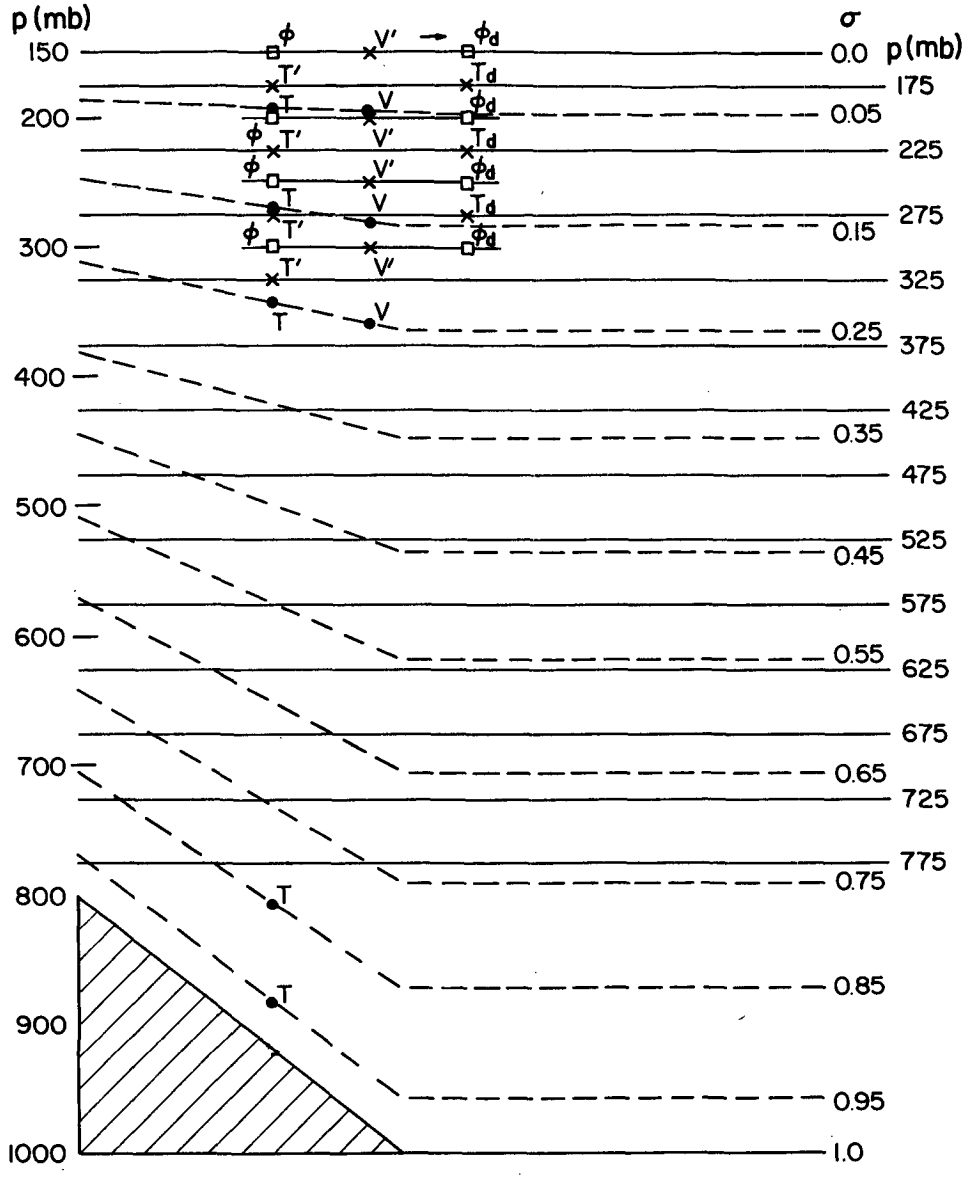

FIG. 1. Vertical grid structure of OSSE. The dashed lines are the model σ-levels at which the temperature T and wind components V are defined. The straight solid lines are constant-pressure levels at which the interpolated model temperatures T' and the temperatures T_d derived from the divergence equation are defined (175, 225, · · · 775 mb). The interpolated velocity components V' and the derived geopotentials ϕ_d are defined on the constant-pressure surfaces 150, 200, 250, · · · mb.

hydrostatic equation is then used to calculate the temperatures, and these derived temperatures are compared to the temperatures in the model data set, which are assumed to be free of error.

c. *Computational procedure*

The computational procedure is summarized by the following steps.

1) The model wind components from the ten model σ-levels are interpolated to constant pressure surfaces spaced 50 mb apart (150, 200, · · · 1,000 mb; see Fig. 1). The wind components at 150 mb are obtained by extrapolation. The wind components below ground are set to zero.

2) Two passes of a 1-2-1 smoothing operator are applied in the horizontal to eliminate any $2\Delta s$ noise, where Δs is the grid size (50 km).

3) The vertical motion ω is calculated from the horizontal divergence using the kinematic method with $\omega = 0$ at the upper and lower boundaries (150 and 1,000 mb) following O'Brien's (1970) technique.

4) All terms on the left side of (4) are calculated using centered differences.

5) The model temperatures are interpolated from the ten model σ-levels to constant pressure levels located halfway between the levels at which winds are defined (175, 225, $\cdots$ 975 mb) and smoothed lightly in the horizontal. The temperatures at 175 mb are obtained by extrapolation (Fig. 1). The temperatures below ground are extrapolated from the lower model level using the standard lapse rate (6.5 K km^{-1}).

6) The geopotential ϕ is calculated on the lateral boundaries at each constant pressure level (150, 200, $\cdots$ 1,000 mb) from the interpolated temperatures T' by integrating the hydrostatic equation downward from 150 mb, the top σ-level in the model (Fig. 1).

7) The ϕ_d on the interior is calculated from (4) using the forcing function (step 4) and the values of ϕ on the lateral boundaries.

8) The derived temperatures T_d are calculated from the derived values of ϕ_d using the hydrostatic equation.

9) The rms differences between derived and true temperatures and geopotentials are computed.

There are three sources of error in the above procedure. The first is the neglect of the frictional terms F_u and F_v in the diagnostic calculation. Presumably, these terms are most important in the PBL of the model and on the smallest scales, where the ∇^4 terms are large. The second source of error is the vertical interpolation of the model data from σ to pressure levels, as well as the several interpolations necessary to obtain derived and true estimates of temperature and geopotential at the same levels (for verification). Finally, truncation errors are introduced in the calculations of the spatial and temporal derivatives on the left side of (4).

3. Results

The results from 11 OSSEs are summarized in Table 1. The calculations are carried out at 12 h of the model simulation. The rms errors of temperature and height are computed over 13 pressure levels (175, 225, $\cdots$ 775 mb for temperature, and 200, 250, $\cdots$ 800 mb for height). The lower levels are not included because of higher uncertainties associated with extrapolation below ground. Experiment 1 is the control; it utilizes the full data set at highest resolution in time and space with perfect values of ϕ specified as the boundary condition. The errors in this case result only from the three sources discussed in Section 2c. They represent the inherent errors associated with this retrieval technique with the resolution shown in Fig. 1. If perfect observations were available on isobaric surfaces so that vertical interpolation were not necessary, these errors could be reduced. It is noteworthy that the rms temperature errors of 0.64°C are considerably less than those reported by Anthes and Keyser (1979) and are comparable to instrument errors associated with radiosondes (Kuo and Anthes, 1984a). The rms height errors of ~4 m are considerably smaller than the differences between operational analyses of geopotential heights, which are ~20 m at 500 mb (Baumhefner, 1984; Hollingsworth *et al.*, 1985).

Figures 2 and 3 show the derived temperatures at 725 mb from Experiment 1 and the differences from the true temperatures at this level. As suggested by

TABLE 1. Summary of Observing Systems Simulation Experiments.

Experiment	Horizontal resolution	Temporal resolution (h)	Superimposed error ($m\ s^{-1}$)	Equation	rms errors: Temperature (°C)	rms errors: Height (m)
1	50	0.17	0	divergence	0.64	4.0
2	50	1	0	divergence	0.65	4.1
3	50	1	0	balance	1.22	6.4
4	200	1	0	divergence	0.59	4.0
5	350	1	0	divergence	0.79	4.5
6	250*	1	0	divergence	1.62	6.0
7	200	1	1	divergence	0.86	4.2
8	350	1	1	divergence	0.96	4.8
9	250*	1	1	divergence	1.97	6.9
10	350	1	1 (plus errors on boundary values of geopotential)	divergence	1.00	11.1
11	350	1	1 (plus systematic errors of geopotential on boundaries)	divergence	1.55	18.8

* Irregular grid.

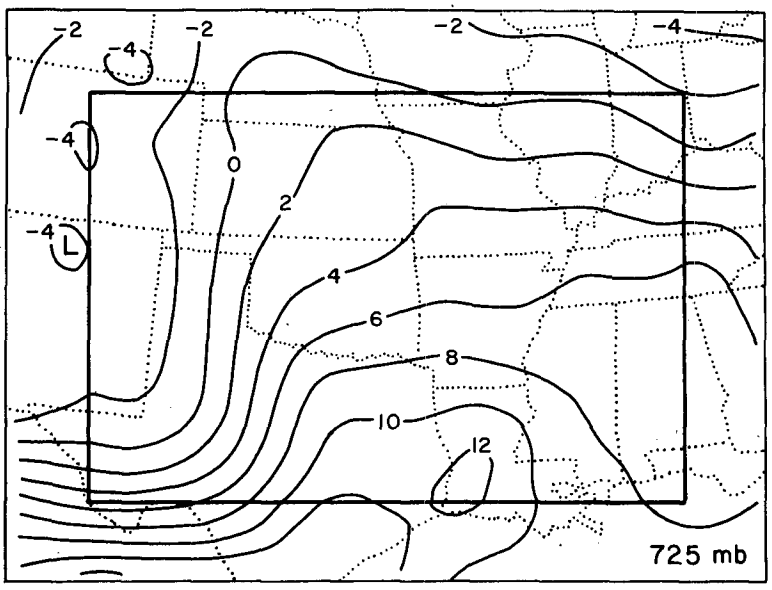

FIG. 2. Temperatures (°C) derived from the divergence equation at 725 mb (interior region) for Experiment 1. Temperatures outside the interior region are the model temperatures.

the rms errors, the errors at most points are less than 1°C. However, systematic errors of greater than 1°C exist over western Texas, Oklahoma, and parts of Colorado and Kansas. These temperature errors and the associated errors in static stability could be important in numerical forecasts of convective systems.

Figures 4, 5, and 6 illustrate the quality of the derived heights. The important features of the true height field (Fig. 4), including the diffluent flow over Oklahoma, are well represented by the derived heights (Fig. 5). The height errors are generally less than 10 m (Fig. 6).

The results from Experiment 1 indicate that useful height and temperature data can be derived from high-resolution wind data. The subsequent experiments (Table 1) indicate the way in which a degradation in temporal and horizontal resolution and superposition of errors on the wind observations

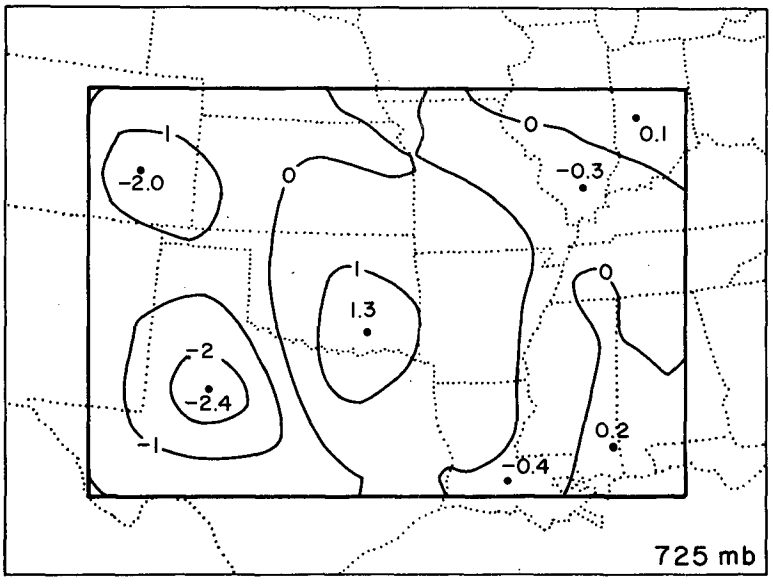

FIG. 3. Difference between derived and model temperatures (°C) from Experiment 1.

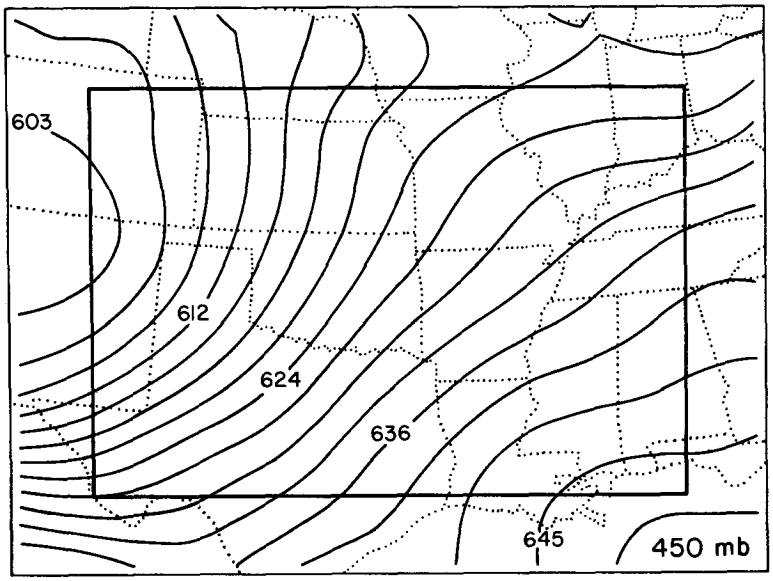

FIG. 4. Model (true) heights of 450-mb surface in decameters.

contribute to increases in height and temperature errors. In addition, a comparison of Experiment 3, in which the balance equation is used rather than the full divergence equation, with Experiment 2 gives an estimate of the value of including the divergence and vertical motion terms in the diagnostic calculation.

Experiment 2, in which data at a time interval of 1 h rather than 10 min are used in the calculation, gives results almost identical to those of Experiment 1. This result is not surprising because the model data set was filtered to remove temporal scales less than 6 h.

The neglect of the divergence and vertical motion terms in Experiment 3 produces a significant increase in rms temperature and height errors. The rms temperature errors double and the rms height errors increase by about 56%. The smaller percentage increase in the height errors indicates that some of the temperature errors cancel in the vertical integration of the hydrostatic equation to compute the heights.

Experiments 4 and 5 investigate the effects of decreased horizontal resolution. In these experiments, the wind data are extracted on a regular grid with separations of 200 or 350 km, then analyzed by a

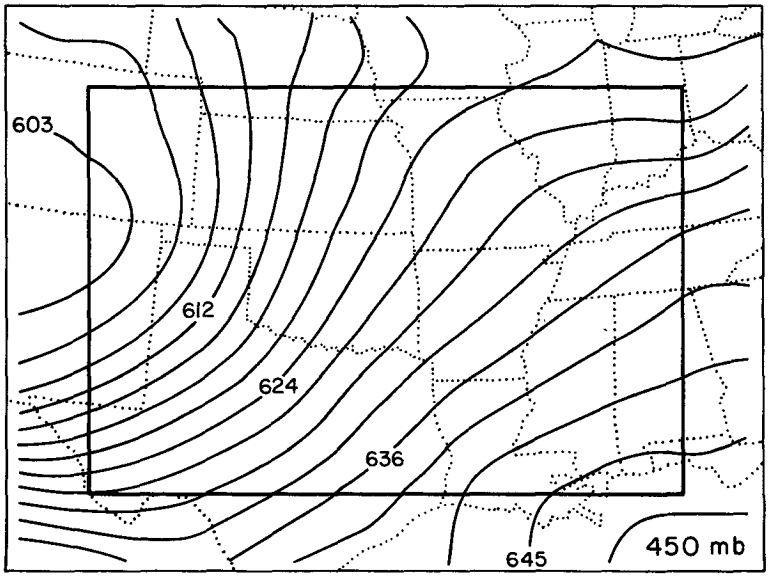

FIG. 5. Derived heights (decameters) of 450 mb surface for Experiment 1 (interior region).

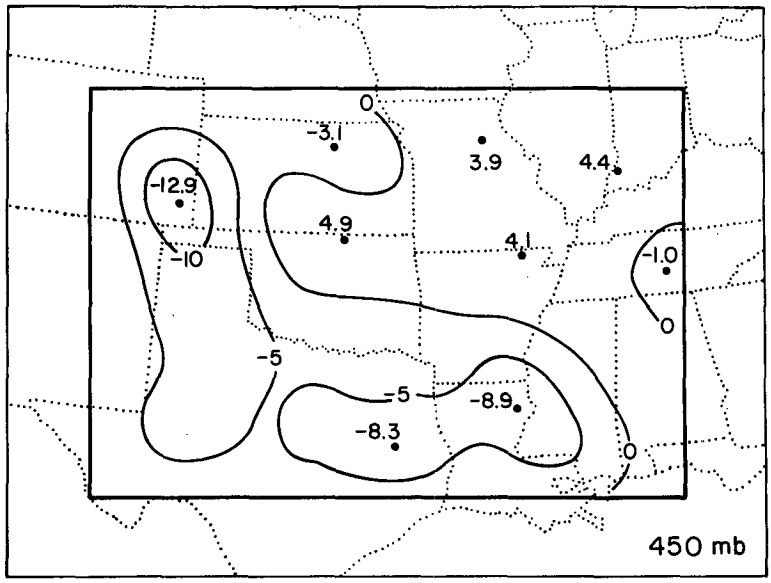

FIG. 6. Difference between derived and model heights (*m*) for Experiment 1 at 450 mb.

cubic-spline technique to the original 50 km grid. The small increase in rms errors in these two experiments indicates that, for this case, the calculations are not sensitive to horizontal resolution when the observations are on a regular mesh.

Observation points are generally spaced irregularly, and objective analysis is needed to obtain estimates of the variables on a regular grid. Ogura and Chen (1977) have shown that even though the variable itself is well analyzed, derived quantities (such as divergence and vorticity) can be very sensitive to the analysis procedure. Experiment 6 investigates the effect of irregularly spaced observations and the necessary objective analysis. In Experiment 6, the model wind components are extracted at the points of the AVE-SESAME-79 network (Alberty *et al.*, 1980) which have an average station separation of 250 km. These data are then analyzed by the Cressman (1959) objective analysis scheme using Experiment 8 as the first guess. The rms errors for Experiment 6 are 1.62°C for temperature and 6.0 m for the geopotential height. The rms temperature errors are twice as large as those of Experiment 5. Figures 7 and 8 show the temperature error at 725 mb and

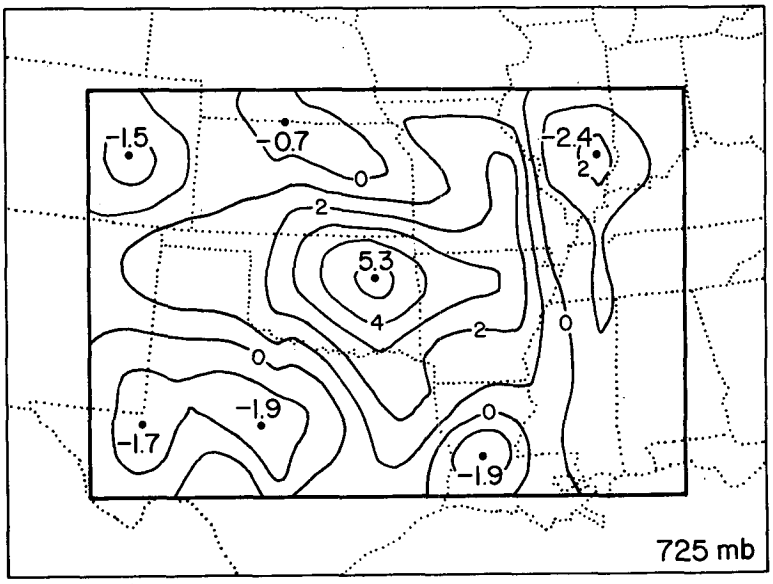

FIG. 7. Difference between derived and model temperatures (°C) at 725 mb for Experiment 6.

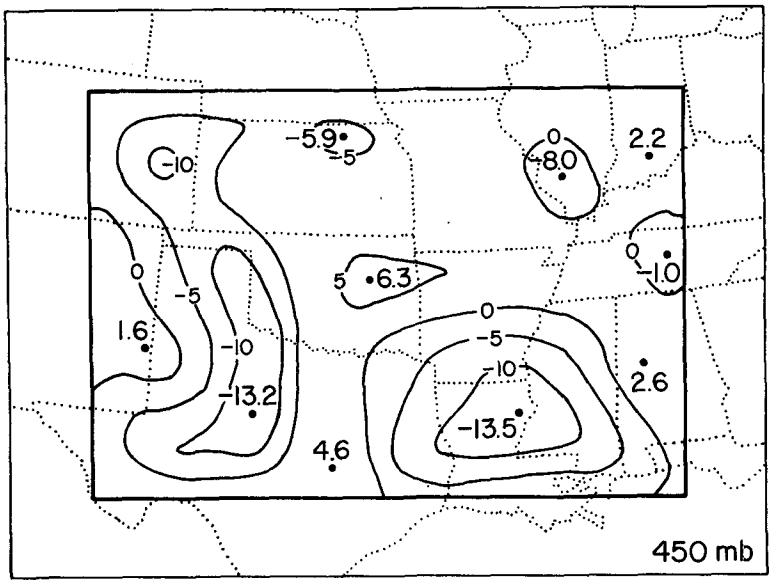

FIG. 8. As in Fig. 6 but for Experiment 6.

height error at 450 mb for this experiment. Over the area of strong convection in Oklahoma the temperature error is 5.3°C. These results suggest that accurate divergence and vertical motions are much more difficult to estimate when wind observations are placed irregularly.

Experiments 7 and 8 investigate the effect of adding random errors (rms errors of 1 m s^{-1}) to the wind observations at 200 and 350 km resolutions. As expected, the greatest errors occur for the coarse resolution (Experiment 8). Figure 9 shows the temperature errors at 725 mb for Experiment 8. In spite of the wind errors, it is apparent that useful temperature information can still be derived from the divergence equation. A somewhat worse situation exists at 425 mb (Fig. 10), however, where temperature errors exceed 3.5°C over eastern Oklahoma and over parts of Arkansas, Louisiana and Mississippi. These are regions of strong moist convection and latent heating in the numerical simulation, and the divergent wind components and vertical motion are large here. Therefore, the errors due to vertical interpolation of these quantities are probably larger here than in other portions of the domain.

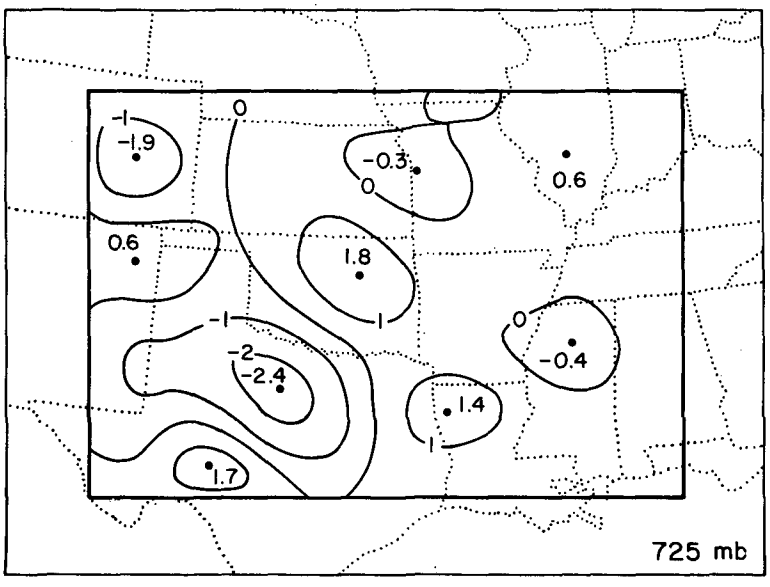

FIG. 9. As in Fig. 7 but for Experiment 8.

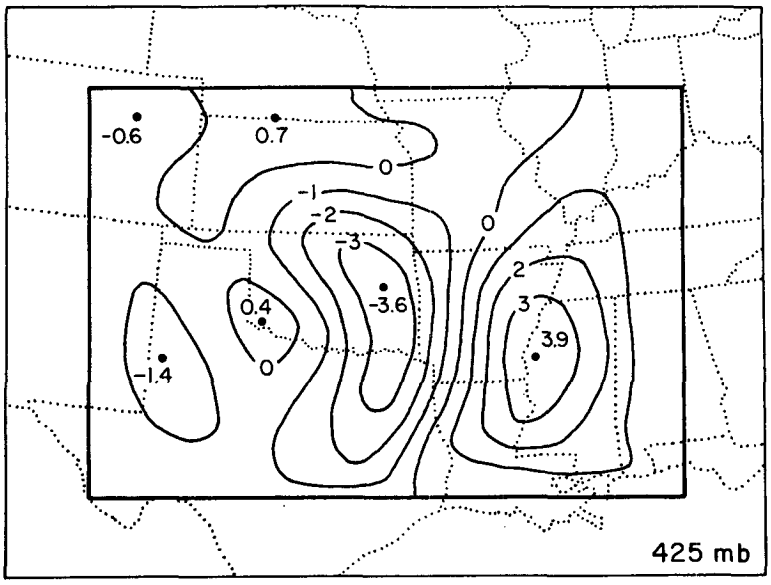

FIG. 10. Difference between derived and model temperatures (°C) at 425 mb for Experiment 8.

The height errors at 450 mb for Experiment 8 are shown in Fig. 11. In spite of the relatively large temperature errors at some points and some levels, the maximum height errors are less than 20 m everywhere. This indicates that a significant fraction of the temperature error is uncorrelated in the vertical (Fig. 12) and cancels in the vertical integration of the hydrostatic equation. This suggests that filtering the derived temperature profiles in the vertical may reduce the rms temperature errors.

The effects of adding random errors to the wind observations on the irregular mesh of Experiment 6 were investigated in Experiment 9. The rms errors in temperature and geopotential height are increased, compared to the errors in Experiment 6, to 1.97°C and 6.9 m, respectively. The general pattern and magnitude of the temperature and height errors for Experiment 9 (not shown) are similar to those in Experiment 6 (Figs. 7 and 8). A comparison of the results of Experiments 7, 8 and 9 indicates that the effects of random wind errors are larger when observations are available at irregular points than when they are available on a regular mesh.

In the above calculations, the true values of the

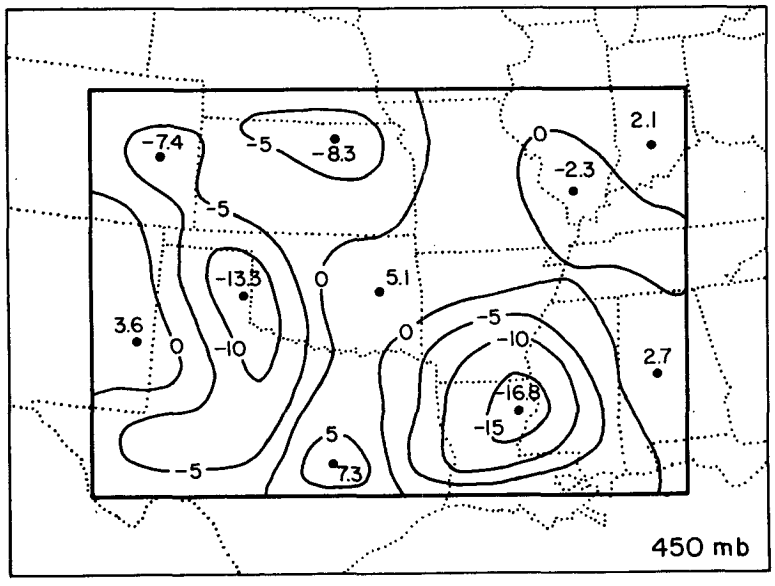

FIG. 11. As in Fig. 6 but for Experiment 8.

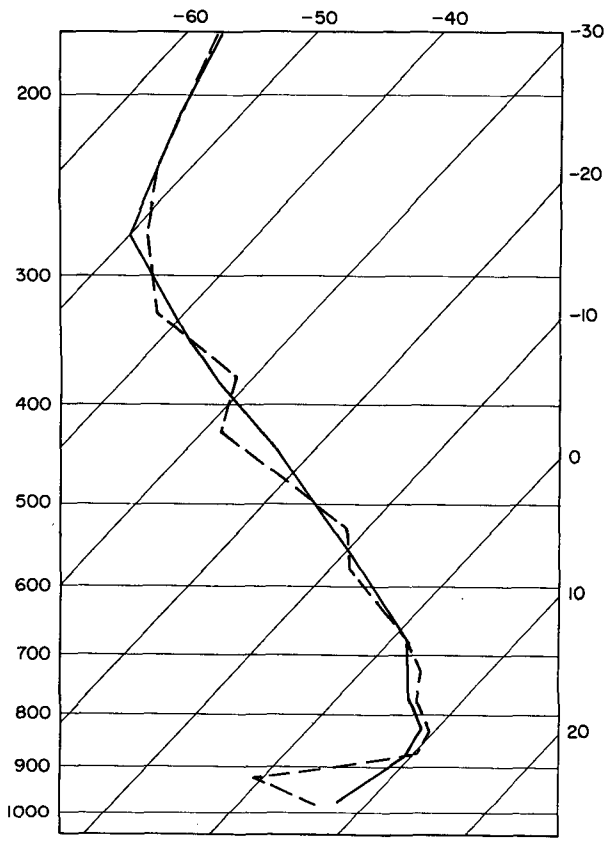

FIG. 12. Vertical profiles of model (solid) and derived (dashed) temperatures from Experiment 2 at a point over northeastern Oklahoma.

geopotentials serve as the boundary conditions in the solution of the divergence equation. In an operational configuration, the boundary conditions have to be estimated from either radiosonde and satellite observations or from a numerical model forecast, and they are likely to contain a certain amount of systematic and random errors. To test the sensitivity of the derived temperature and geopotential fields to errors on the lateral boundaries, a degraded temperature field is first created by adding 0.5°C (in an rms sense) temperature perturbations to an array of model temperatures with 350 km spacing. The contaminated observations are then analyzed and integrated to obtain a degraded geopotential field. When averaged over 13 levels, the degraded geopotentials contain an rms error of 8.0 m. Experiment 10 is then carried out with conditions identical to those of Experiment 8, except that the boundary conditions are specified from the degraded geopotential field. The rms errors of Experiment 10 are 1.0°C in temperature and 11.1 m in geopotential height (Table 1). The rms differences between Experiment 10 and 8, which are a measure of the errors introduced by errors in the lateral boundary conditions, are 0.47°C in temperature and 8.8 m in geopotential height. Figures 13 and 14 show the difference of temperature and geopotential fields between Experiment 10 and 8. As expected, major differences exist near the boundaries, but these differences decrease rapidly away from them, in agreement with the theoretical analysis of Anthes and Keyser (1979). This suggests that useful estimates of temperature and geopotential can still be obtained despite

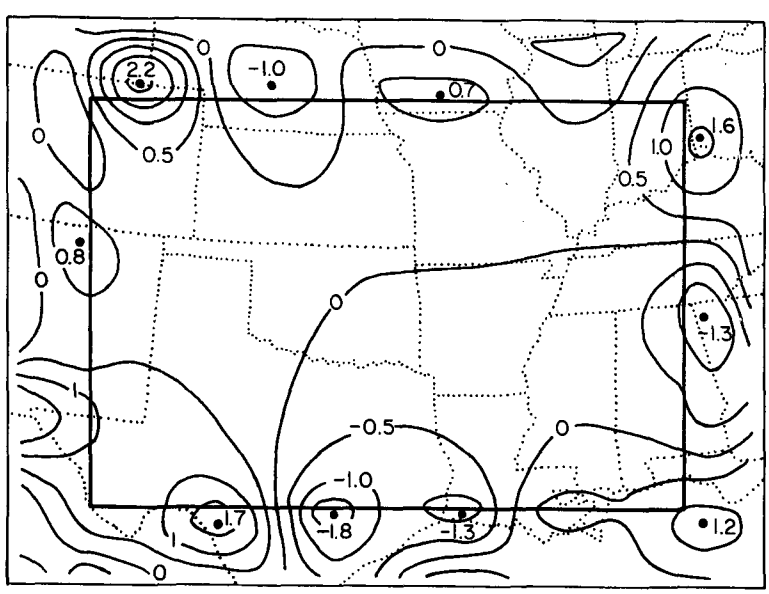

FIG. 13. Difference between derived temperatures (°C) in Experiment 10 and 8 at 725 mb. The difference outside the interior region represents the specified temperature "errors"; the differences over the interior region represent the effect of the erroneous boundary conditions.

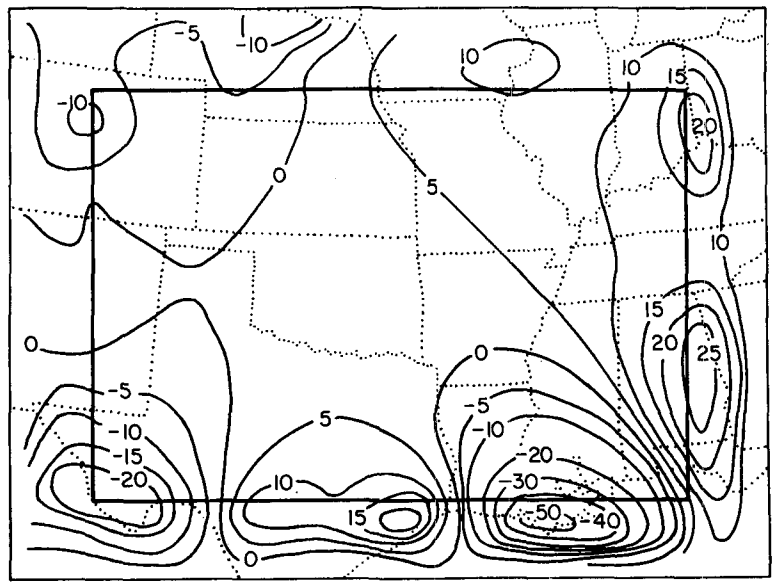

FIG. 14. Differences in height (m) of the 450 mb surface between Experiments 10 and 8. The differences outside the interior region represent the error due to the specified temperature errors; the differences over the interior region illustrate the effect of the erroneous boundary conditions.

the existence of random errors in geopotential height at the boundary.

In an operational system, the boundary conditions in geopotential height could be obtained from a large-scale model's forecast temperatures. The forecast temperature errors are likely to be more highly correlated in the vertical than are the random errors superimposed in Experiment 10. Experiment 11 investigates the effects of such systematic errors in the boundary values of geopotential height. In this experiment, an analysis of geopotential height is obtained from the AVE-SESAME-79 temperature observations (Kuo and Anthes, 1984a). The rms differences of observed versus model heights and temperatures are 25.6 m and 1.93°C, respectively, averaged over 13 levels. These values represent the forecast errors of this particular simulation and are slightly less than the typical errors of regional-scale models as reviewed by Anthes (1983). Experiment 11 is then carried out with conditions identical to those of Experiment 8, except that the boundary conditions are specified from the observed rather than the model geopotential heights. The results of Experiment 11 are shown in Figs. 15 and 16. Owing to the forecast temperature errors, the model geopotential heights on the boundary may be systematically higher (or lower) than the observed heights, and this error results in a positive (or negative) bias error over the whole domain. The rms errors for Experiment 11 are 1.55°C and 18.8 m, compared to 0.96°C and 4.8 m for Experiment 8. These results indicate that systematic errors in the boundary conditions contribute significant errors to the derived temperatures on the interior. Independent temperature observations from radiosondes, satellites, or from temperature profilers are needed to provide accurate estimates of geopotential height for the boundary conditions.

As discussed before, some of the temperature errors are not correlated in the vertical; they can be suppressed by a light vertical smoothing. To illustrate the effect of vertical smoothing, a simple 1–2–1 smoother is applied to the derived temperature field of Experiment 11. The results showed slight improvement. The rms error averaged over 13 levels was reduced from 1.55 to 1.36°C.

4. Summary

Observing systems simulation experiments indicate that useful estimates of temperature can be derived from high-resolution wind observations such as those that might be obtainable from a wind profiling system. Adding the divergence and vertical motion terms to the balance equation to form the complete divergence equation reduces the errors in derived temperatures and heights. Observations on an irregularly spaced grid lead to greater errors than those on a regularly spaced one. Significant errors are introduced when systematic errors in geopotential are provided as lateral boundary conditions. Vertical smoothing is effective in suppressing some of the temperature errors.

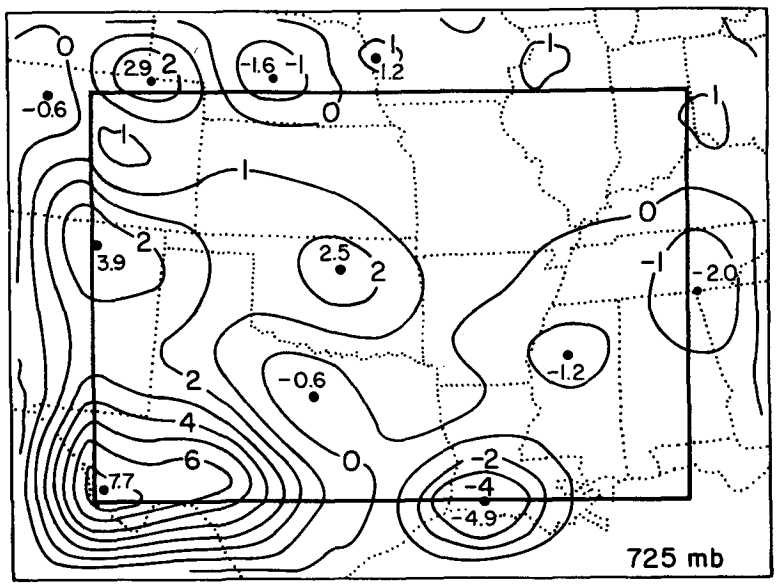

FIG. 15. Difference between model and derived temperatures (°C) at 725 mb for Experiment 11. The differences outside the interior region represent the systematic error in temperature; the differences over the interior region illustrate the effect of systematic errors in the boundary conditions plus random errors in the wind observations.

The above conclusions probably depend somewhat on the vertical resolution of the model (10 layers in this study). Further studies should employ a higher-resolution model with the retrieval technique directly applied on the constant σ-levels to avoid vertical interpolations. Further model simulations should also be carried out to test the usefulness of the derived temperature fields in initializing numerical models along with the wind fields obtained from a wind profiler system.

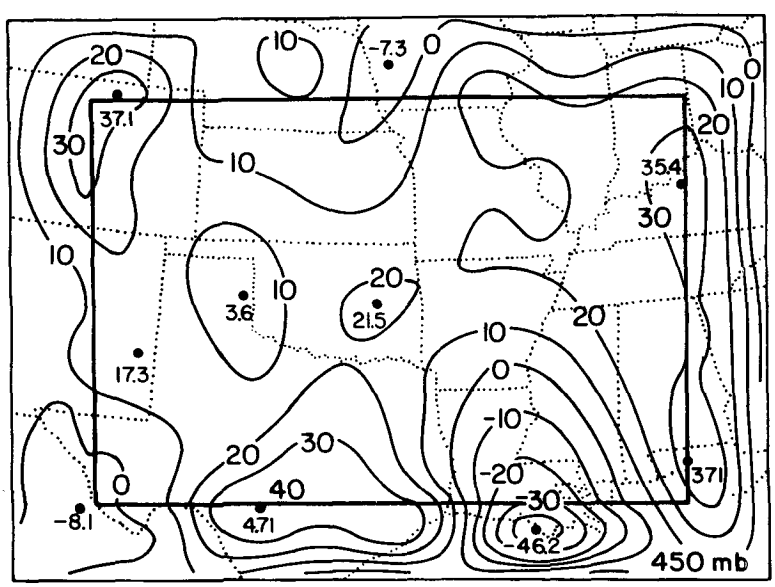

FIG. 16. Difference between model and derived heights (m) at 450 mb for Experiment 11. The differences outside the interior region represent the systematic error in height; the differences over the interior region are as in Fig. 15.

Acknowledgments. We thank Roger Daley, David Baumhefner, Akira Kasahara, Melvyn Shapiro, and two anonymous reviewers for their helpful comments.

Ann Modahl provided excellent assistance in editing and typing the manuscript.

REFERENCES

Alberty, R. L., D. W. Burgess and T. T. Fujita, 1980: Severe weather events of 10 April 1979. *Bull. Amer. Meteor. Soc.*, **61,** 1033–1034.

Anthes, R. A., 1983: Regional models of the atmosphere in middle latitudes. *Mon. Wea. Rev.*, **111,** 1306–1335.

——, and D. Keyser, 1979: Tests of a fine-mesh model over Europe and the United States. *Mon. Wea. Rev.*, **107,** 963–984.

——, Y.-H. Kuo, S. G. Benjamin and Y.-F. Li, 1982: The evolution of the mesoscale environment of severe local storms: Preliminary modeling results. *Mon. Wea. Rev.*, **110,** 1187–1213.

Baumhefner, D. P., 1984: Analysis and forecast intercomparisons using the FGGE SOP1 data base. Paper presented at the NAS FGGE Workshop.

Bleck, R., R. Brummer and M. A. Shapiro, 1984: Enhancement of remotely sensed temperature fields by wind observations from a VHF radar network. *Mon. Wea. Rev.*, **112,** 1795–1803.

Cressman, G. P., 1959: An operational objective analysis system. *Mon. Wea. Rev.*, **87,** 367–381.

Fankhauser, J. C., 1974: The derivation of consistent fields of wind and geopotential height from mesoscale rawinsonde data. *J. Appl. Meteor.*, **13,** 637–646.

Hogg, D. C., M. T. Decker, F. O. Guiraud, K. B. Garnshaw, D. A. Merritt, K. P. Moran, W. B. Sweezy, R. G. Strauch, E. R. Westwater and C. G. Little, 1983: An automatic profiler of the temperature, wind and humidity in the troposphere. *J. Climate Appl. Meteor.*, **22,** 807–831.

Hollingsworth, A., A. C. Lorenc, M. S. Tracton, K. Arpe, G. Cats, S. Uppala and P. Kallberg, 1985: The response of numerical weather prediction systems to FGGE level II-b data. Part I: Analysis. *Quart. J. Roy. Meteor. Soc.*, **111**(No. 467), 1–66.

Hovermale, J. B., 1983: Summary of a workshop on atmospheric profiling, 3–4 March, Boulder, CO. *Bull. Amer. Meteor. Soc.*, **64,** 1062–1066.

Kuo, Y.-H., and R. A. Anthes, 1984a: Accuracy of diagnostic heat and moisture budgets using SESAME-79 field data as revealed by observing system simulation experiments. *Mon. Wea. Rev.*, **112,** 1465–1481.

——, and ——, 1984b: Mesoscale budgets of heat and moisture in a convective system over the central United States. *Mon. Wea. Rev.*, **112,** 1482–1497.

O'Brien, J. J., 1970: Alternative solutions to the classical vertical velocity problem. *J. Appl. Meteor.*, **9,** 197–203.

Ogura, Y., 1975: On the interaction between cumulus clouds and the larger-scale environment. *Pure Appl. Geophys.*, **113,** 869–889.

——, and Y. Chen, 1977: A life history of an intense mesoscale convective storm in Oklahoma. *J. Atmos. Sci.*, **34,** 1458–1476.

Shapiro, M. A., D. C. Hogg and C. G. Little, 1983: The wave propagation laboratory profiler system and its applications. *Proc. Fifth Symposium on Meteorological Observations and Instrumentation,* Toronto, Amer. Meteor. Soc., 174–182.

Strauch, R. G., D. A. Merritt, K. P. Moran, K. B. Earnshaw and D. van de Kamp, 1984: The Colorado wind-profiling network. *J. Atmos. Oceanic Technol.*, **1,** 37–49.

Zamora, R. J., and M. A. Shapiro, 1984: Diagnostic divergence and vorticity calculations using a network of mesoscale wind profilers. *Proc. Tenth Conf. Weather Forecasting and Analysis,* Clearwater Beach, Amer. Meteor. Soc., 386–391.